Early retinal neurodegeneration and impaired Ran-mediated nuclear import of TDP-43 in progranulin-deficient FTLD

Michael E. Ward,[1,2] Alice Taubes,[1] Robert Chen,[2] Bruce L. Miller,[2] Chantelle F. Sephton,[5] Jeffrey M. Gelfand,[2] Sakura Minami,[1] John Boscardin,[3] Lauren Herl Martens,[4] William W. Seeley,[2] Gang Yu,[5] Joachim Herz,[5] Anthony J. Filiano,[6] Andrew E. Arrant,[6] Erik D. Roberson,[6] Timothy W. Kraft,[7] Robert V. Farese, Jr.,[4] Ari Green,[2] and Li Gan[1,2]

[1]Gladstone Institute of Neurological Diseases, [2]Department of Neurology, [3]Department of Medicine, [4]Gladstone Institute of Cardiovascular Disease, University of California, San Francisco, San Francisco, CA 94158
[5]Department of Neuroscience, University of Texas Southwestern Medical Center, Dallas, TX 75390
[6]Departments of Neurology and Neurobiology and [7]Department of Vision Sciences, University of Alabama at Birmingham, Birmingham, AL 35294

Frontotemporal dementia (FTD) is the most common cause of dementia in people under 60 yr of age and is pathologically associated with mislocalization of TAR DNA/RNA binding protein 43 (TDP-43) in approximately half of cases (FLTD-TDP). Mutations in the gene encoding *progranulin* (*GRN*), which lead to reduced progranulin levels, are a significant cause of familial FTLD-TDP. *Grn*-KO mice were developed as an FTLD model, but lack cortical TDP-43 mislocalization and neurodegeneration. Here, we report retinal thinning as an early disease phenotype in humans with *GRN* mutations that precedes dementia onset and an age-dependent retinal neurodegenerative phenotype in *Grn*-KO mice. Retinal neuron loss in *Grn*-KO mice is preceded by nuclear depletion of TDP-43 and accompanied by reduced expression of the small GTPase Ran, which is a master regulator of nuclear import required for nuclear localization of TDP-43. In addition, TDP-43 regulates Ran expression, likely via binding to its 3′-UTR. Augmented expression of Ran in progranulin-deficient neurons restores nuclear TDP-43 levels and improves their survival. Our findings establish retinal neurodegeneration as a new phenotype in progranulin-deficient FTLD, and suggest a pathological loop involving reciprocal loss of Ran and nuclear TDP-43 as an underlying mechanism.

CORRESPONDENCE
Ari Gree:
agreen@ucsf.edu
OR
Li Gan:
lgan@gladstone.ucsf.edu

Abbreviations used: AD, Alzheimer's disease; CDR, clinical disease rating; FTD, frontotemporal dementia; FTLD, frontotemporal lobar degeneration; GCC, ganglion cell complex; *GRN*, *progranulin*; INL, inner nuclear layer; OCT, optical coherence tomography; ONL, outer nuclear layer; PD, Parkinson's disease; PSP, progressive supranuclear palsy; RGC, retinal ganglion cell; RNFL, retinal nerve fiber layer; PhNR, photopic negative response; TDP-43, TAR DNA/RNA binding protein 43.

Approximately 50% of (frontotemporal dementia) FTLD cases are characterized by cellular aggregation and mislocalization of TDP-43 (i.e., FTLD-TDP). TDP-43 normally localizes to the nucleus and regulates transcriptional control, splicing, and RNA processing (Sephton et al., 2011; Polymenidou et al., 2011). In FTLD-TDP, nuclear depletion of TDP-43 occurs, often in neurons containing cytoplasmic TDP-43 aggregates (Neumann et al., 2006). The mechanisms underlying TDP-43 mislocalization in FTLD have not been characterized, and whether TDP-43 mislocalization plays a causal role in neurodegeneration remains controversial (Lee et al., 2012). FTLD has sporadic and familial forms. Mutations in the *GRN* gene that cause progranulin haploinsufficiency are a common cause of familial FTLD-TDP (Baker et al., 2006). Aged *Grn*-KO mice exhibit FTD-like behavioral abnormalities but lack TDP-43 mislocalization or neurodegeneration in cortical regions (Ahmed et al., 2010; Yin et al., 2010; Martens et al., 2012).

Retinal abnormalities are documented in Alzheimer's disease (AD), progressive supranuclear palsy (PSP), Parkinson's disease, and multiple systems atrophy (Hinton et al., 1986; Bayer et al., 2002; Tamura et al., 2006; Paquet et al., 2007; Albrecht et al., 2012; Helmer et al., 2013).

The Rockefeller University Press $30.00
J. Exp. Med. 2014 Vol. 211 No. 10 1937-1945
www.jem.org/cgi/doi/10.1084/jem.20140214

Due to the clinical accessibility of the retina, new retinal imaging techniques under development hold promise as potential diagnostic and prognostic modalities for neurodegenerative diseases (Koronyo-Hamaoui et al., 2011). However, whether retinal abnormalities are an early or late disease phenomenon has not been established. Here, we identify retinal neurodegeneration as a novel disease-related phenotype in human subjects with *GRN* mutations before clinical symptoms of dementia. In *Grn*-KO mouse, retinal neuronal loss is preceded by depletion of nuclear TDP-43. We further explore the role of Ran, a central regulator of nuclear trafficking, in TDP-43 nuclear depletion and degeneration in *Grn*-KO neurons. Our findings suggest a novel relationship between TDP-43 and Ran-mediated nuclear trafficking in FTLD pathogenesis.

RESULTS AND DISCUSSION

Early retinal abnormalities in humans with *GRN* mutations and *Grn*-KO mice

Because retinal neuron loss occurs in other neurodegenerative diseases, we suspected that retinal neurons could be a vulnerable neuronal population in humans with progranulin haploinsufficiency secondary to *GRN* mutations. Using optical coherence tomography (OCT), we measured retinal nerve fiber layer (RNFL) thickness and macular volume in living human control subjects and subjects with *GRN* mutations. The RNFL constitutes the axonal compartment of retinal ganglion cells (RGCs) and, as such, is a surrogate measurement of RGC number. Macular volume is a combined measurement of all of the layers of the retina within the macula. We observed significant reductions in RNFL thickness and macular volume in subjects with *GRN*

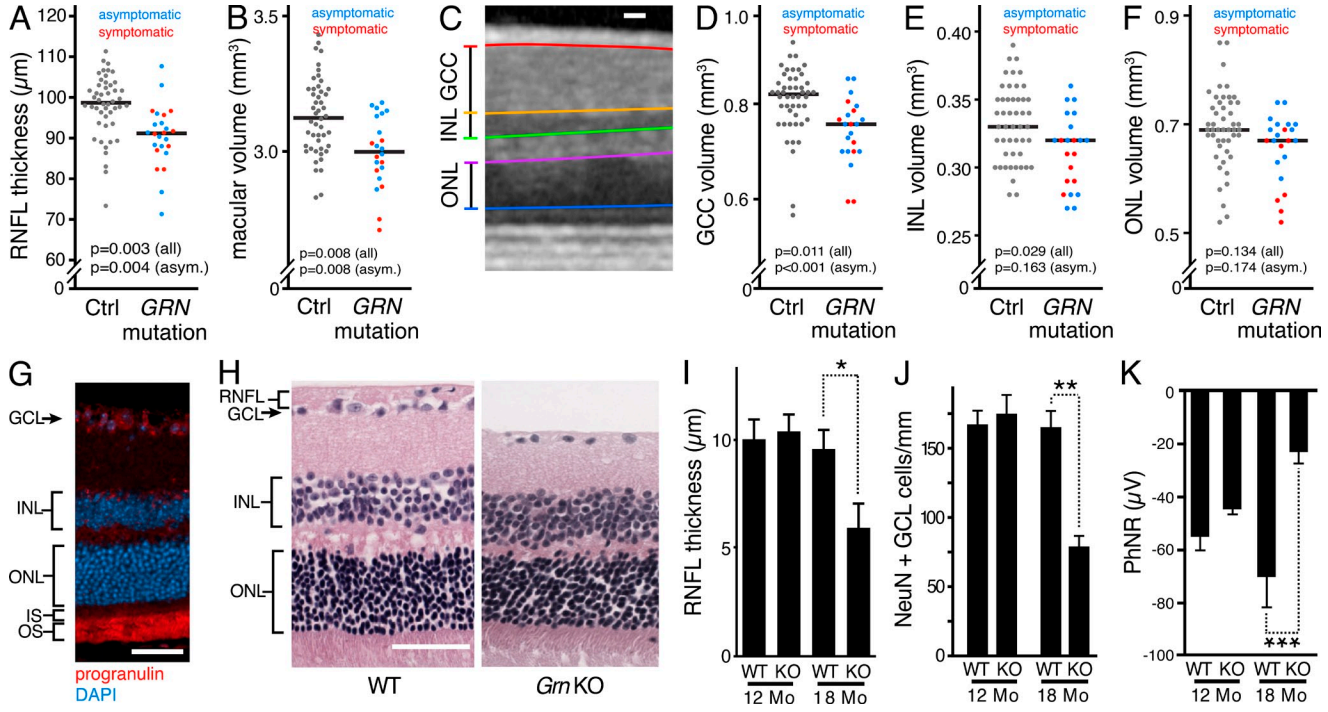

Figure 1. Progranulin deficiency causes retinal neuron loss in humans with *GRN* mutations and retinal neuron loss/dysfunction in a progranulin-deficient mouse model of familial FTLD. (A and B) RNFL thinning (A) and macular volume loss (B) occur in humans with progranulin haploinsufficiency caused by *GRN* mutations and precede dementia onset. Each dot represents value of an individual eye, and bars represent median values. Asymptomatic *GRN*-mutation carriers (CDR = 0) are shown in blue and symptomatic *GRN* mutation carriers (CDR score ≥ 0.5) are shown in red. Control age- and sex-matched subjects are represented by gray dots. (C–F) Macular ganglion cell loss occurs in *GRN* mutation carriers and precedes dementia onset. An automated segmentation algorithm (C) was used to determine the volumes of GCC (D), INL (E), and ONL (F) in the maculae of control and *GRN* mutation carriers (D–F). Results represent a single cohort of $n = 24$ control subjects and 12 *GRN* mutation carrier subjects (7 asymptomatic, 5 symptomatic), and p-values were generated via mixed-effects linear regression analyses. (G) Progranulin expression occurs in the GCL and photoreceptor inner and outer segments (IS, OS) of mouse retinas. Immunostaining of progranulin and DAPI staining of nuclei are shown in a representative retinal cross section. (H) RNFL thinning and loss of inner retinal neurons shown in H&E-stained retinal cross sections from 18-mo-old *Grn* KO mice. Representative sections equidistant to the optic nerve are shown. (I) Quantification of RNFL layer thickness. $n = 5$–7 mice/age/genotype; *, $P < 0.05$, one-way ANOVA with Tukey's post-hoc analysis, 2 independent experiments. (J) Loss of Neu-N–positive neurons in the GCL of 18-mo *Grn* KO retinas. Neu-N–positive cells in the GCL were quantified in sections equidistant to the optic nerve head. $n = 5$–7 mice/age/genotype; **, $P < 0.01$, one-way ANOVA with Tukey's post-hoc analysis, 2 independent experiments. (K) Impaired light-evoked RGC electrophysiological responses in aged *Grn* KO mice. Electroretinograms (ERGs) were performed on 12- and 18-mo-old mice, and the amplitude of the photopic-negative response (PhNR, a RGC-specific waveform) was quantified. $n = 6$ mice/age/genotype; ***, $P < 0.001$ at 18 mo of age via repeated measures two-way ANOVA with Bonferroni's multiple comparison test; 2 independent experiments. Bars: (C, G, and H) 50 µm.

mutations compared with controls, indicating that retinal neuron loss occurred in these subjects (Fig. 1, A and B; and Fig. S1). A substantial number of the *GRN* mutation carriers enrolled in our trial (7/12) were cognitively asymptomatic. Intriguingly, we found that this subgroup of asymptomatic *GRN* mutation carriers also had significant reductions in RNFL thickness and macular volume (Fig. 1, A and B). We then analyzed individual neuronal layers of the macula via an automated segmentation algorithm, to determine the volumes of the ganglion cell complex (GCC), inner nuclear layer (INL), and outer nuclear layer (ONL) in the maculae of control and *GRN*-mutation carriers (Fig. 1 C). Significant thinning of the GCC and INL, but not ONL, was observed in *GRN* mutation carriers (Fig. 1, D–F). The volume of GCC was significantly reduced even in asymptomatic carriers, further implicating RGC loss as an early neurodegenerative phenotype in subjects with progranulin deficiency (Fig. 1 D).

We then determined if a similar phenotype occurred in *Grn*-KO mice. Total retinal progranulin expression levels were similar to those in the brain, based on ELISA (unpublished data), with prominent expression in RGCs and photoreceptors (Fig. 1 G). Despite a lack of significant neurodegeneration in the brain (Ahmed et al., 2010; Yin et al., 2010), we observed progressive, substantial thinning of the RNFL and a loss of ganglion cell layer (GCL) cells in 18-mo-old *Grn*-KO mice (Fig. 1, H–J). In agreement with the pathological alterations, electrophysiological abnormalities in *Grn*-KO mouse retinas paralleled GCL neuron loss. At 18 mo, but not 12 mo, of age, *Grn*-KO mice had substantially reduced amplitudes of photopic negative responses (PhNRs), a measure of RGC function (Fig. 1 K). Amplitudes of a- and b-wave responses were also significantly reduced in an age-dependent manner in *Grn*-KO mice, indicating additional dysfunction of inner nuclear layer neurons and photoreceptors (unpublished data).

Nuclear depletion of TDP-43 in *Grn*-KO retinal neurons precedes neurodegeneration

Loss of nuclear TDP-43 is commonly observed in postmortem brain tissue from patients with FTLD-TDP (Neumann et al., 2006; Davidson et al., 2007), including FTLD associated with *GRN* mutations (Fig. 2 A). However, the mechanism of nuclear depletion of TDP-43 in FTLD is unknown, and it remains unclear if loss of nuclear TDP-43 plays a causal role in FTLD pathogenesis. At 18 mo of age, levels of nuclear TDP-43

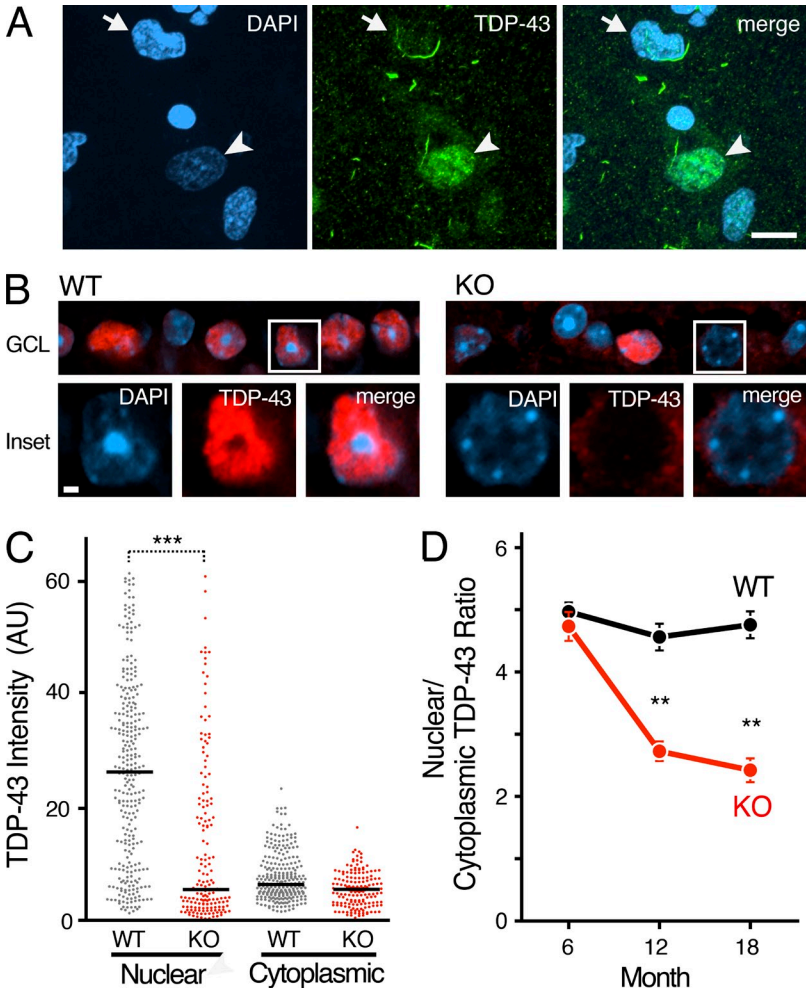

Figure 2. Nuclear depletion of TDP-43 occurs in retinal neurons before neurodegeneration. (A) Postmortem brain tissue from a human *GRN* mutation carrier was co-stained with the nuclear marker DAPI (blue) and an anti–TDP-43 antibody (green). Normal TDP-43 distribution is still observed in some neurons (arrowhead), but other neurons exhibit nuclear depletion of TDP43 (arrow) with or without apparent cytoplasmic inclusions. Bar, 10 µm. (B) Immunofluorescence confocal microscopy of TDP-43 in 18-mo-old retinal GCL neurons. Brightness of the TDP-43 channel was increased in insets to highlight loss of nuclear TDP-43 in *Grn* KO neurons. Bar, 1 µm. (C) Scatter plot of nuclear and cytoplasmic intensities of TDP-43 in GCL neurons of 18-mo-old *Grn* KO mice. n = 121–174 cells from 6 mice/genotype; ***, $P < 0.001$, mixed-effects multivariate linear regression mode; 2 independent experiments. Bars represent median values. (D) Significant reduction in the nuclear/cytoplasmic TDP-43 ratio was observed in 12-mo-old *Grn*-KO GCL neurons (**, $P < 0.01$) and 18-mo-old *Grn*-KO GCL neurons (**, $P < 0.01$). n = 217–357 cells from 5–7 mice/age/genotype, mixed-effects multivariable linear regression model; 2 independent experiments. Mean ± SEM is shown.

were strikingly reduced in *Grn*-KO retinal GCL neurons, whereas levels of cytoplasmic TDP-43 were unchanged (Fig. 2, B and C). Depletion of nuclear TDP-43 also occurred in 12-mo-old *Grn*-KO mice, before significant GCL neuron loss (Fig. 2 D). Interestingly, neither nuclear nor cytoplasmic TDP-43 inclusions were found in the >100 Grn-KO GCL neurons we examined (Fig. 2 B). Thus, in progranulin-deficient FTLD-TDP, nuclear depletion of TDP-43 and neurodegeneration can occur independent of cytoplasmic TDP-43 accumulation/aggregation. These results are consistent with observations that TDP-43, especially nuclear TDP-43, is required for neuron survival (Wegorzewska and Baloh, 2011; Igaz et al., 2011; Arnold et al., 2013).

TDP-43 regulates Ran mRNA levels and requires Ran for nuclear localization

We then explored how nuclear clearing of TDP-43 occurs in FTLD. The small GTPase Ran is a master regulator of nuclear transport (Melchior et al., 1995), and Ran accessory proteins are necessary for nuclear TDP-43 localization (Nishimura et al., 2010). We hypothesized that Ran expression might be altered in our retinal FTLD model and contribute to nuclear TDP-43 depletion. Indeed, nuclear Ran was significantly depleted in *Grn*-KO GCL neurons (Fig. 3, A and B), and nuclear TDP-43 levels correlated with those of nuclear Ran (Fig. 3 C). Moreover, in the inferior frontal gyrus of three patients with FTLD-TDP due to *GRN* mutations, we found a significant correlation between nuclear depletion of TDP-43 and Ran (Fig. 3, D and E).

To understand the mechanisms underlying the intimate correlation between nuclear TDP-43 and Ran, we next assessed whether Ran mRNA is altered in the brains of FTLD-TDP-43 patients, in which TDP-43 is mislocalized. By mining an existing mRNA-expression database comparing healthy control versus *GRN*-mutation-carrying FTD subjects (Chen-Plotkin et al., 2008), we found that cortical Ran expression was reduced by 60% in human subjects carrying a *GRN* mutation ($P = 0.04$). As TDP-43 regulates the expression of thousands of genes, in many cases by binding directly to mRNAs and altering their stability (Polymenidou et al., 2011), we explored the possibility that Ran mRNA is a substrate of TDP-43. Indeed, analyses of a published unbiased screen of the TDP-43–RNA interactions (Sephton et al., 2011) revealed that TDP-43 binds to the 3′ UTR of Ran mRNA (Fig. 4 A). Moreover, inhibiting TDP-43 expression by shRNA-mediated knockdown significantly reduced levels of Ran mRNA (Fig. 4 B) and protein (Fig. 4, C–D) in N2A cells. Ran mRNA levels were also reduced in retinas of aged *Grn* KO mouse (Fig. 4 E), consistent with our observations of nuclear depletion

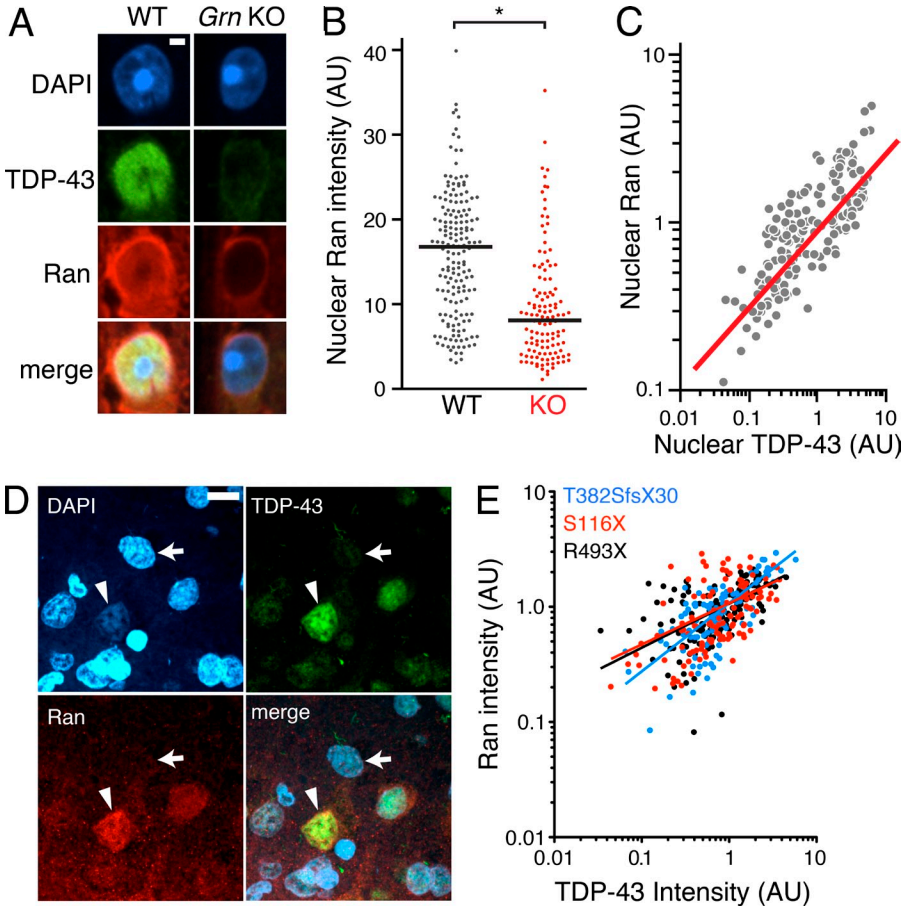

Figure 3. Nuclear clearing of TDP-43 and Ran are pathologically associated in FTLD-TDP. (A) 18-mo-old GCL neurons from WT and *Grn*-KO retinas were co-stained for TDP-43 and Ran. Nuclei were labeled with DAPI. (B) Nuclear Ran levels in 18-mo-old GCL neurons. $n = 165–278$ cells from 6 mice/genotype; *, $P = 0.019$, linear regression model; 2 independent experiments. Scatter plot of individual cell intensities with medians shown. (C) Nuclear Ran and TDP-43 intensities are correlated in *Grn*-KO GCL neurons. Each dot represents a single cell. $n = 165$ cells from 6 *Grn*-KO mice; $r = 0.8963$; $P < 0.001$, Spearman's rho; 2 independent experiments. (D) Immunofluorescence co-staining of *GRN* mutant human cortex shows depletion of Ran and TDP-43 in the same neuron (noted with an arrow; compare to neurons with high levels of TDP-43 and Ran [arrowhead]). (E) TDP-43 and Ran levels correlate in cortical neurons from human *GRN*-mutation carriers. Shown are the correlation analyses of nuclear Ran and TDP-43 intensities of individual neurons from post-mortem brain. $n = 111–141$ cells from each of 3 subjects;, $r = 0.56$; $P < 0.001$. The serum progranulin levels were 19.3–21.2 ng/ml for R493X carrier (control patients: 41.3 ± 15.5 ng/ml). Spearman's rho. Bars: 2 µm (A), 10 µm (D).

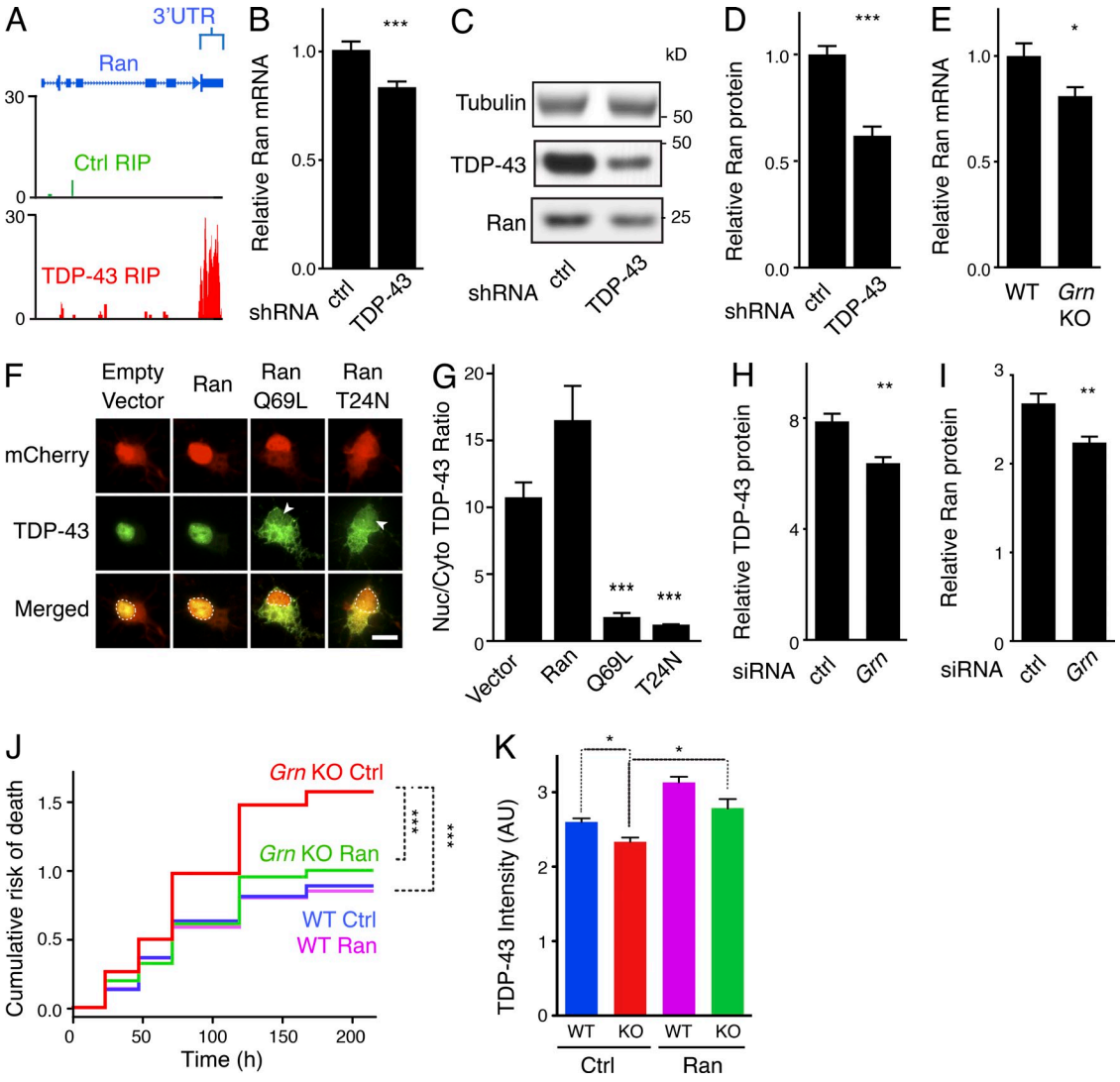

Figure 4. Maintenance of functional TDP-43 and Ran by an interdependent feedback loop and improved survival of *Grn*-KO neurons by exogenous Ran expression. (A) Snapshot of unique reads from the TDP-43 RIP library mapped to the Ran gene shown. Reads mapped to the 3′-UTR of Ran indicate TDP-43 binding. No reads mapped to the Ran gene from the Ctrl RIP library. (B) TDP-43 knockdown in N2A cells results in a reduction in steady-state Ran mRNA levels, as measured by Q-PCR. $n = 12$ wells/group; ***, $P < 0.001$, Student's t test; 3 independent experiments. (C) Representative Western blot showing reduced Ran protein levels after TDP-43 knockdown. (D) Quantification of (C). $n = 9$ wells/group, ***, $P < 0.001$, Student's t test; 2 independent experiments). (E) Ran mRNA expression is reduced in aged *Grn* KO retinas. Q-PCR results from homogenized whole retinas from 10–12-mo-old mice shown. $n = 15$–16 mice/genotype; *, $P = 0.014$; Student's t test; 2 independent experiments. Bars, 10 µm. (F–G) Ran is necessary for nuclear localization of TDP-43. (F) Representative images showing subcellular localization of TDP-43 in cortical neurons cotransfected with TDP-43-GFP and either empty vector, mCherry-Ran, mCherry-RanQ69L, or mCherry-RanT24N. TDP-43-GFP is present in the nuclei of neurons transfected with mCherry and mCherry-Ran, but is significantly reduced in nuclei of neurons transfected with either of the Ran mutants (arrowheads, dashed lines). (G) Quantification of the ratios of nuclear/cytoplasmic TDP-43-GFP. $n = 21$ cells/transfection; ***, $P < 0.001$, one-way ANOVA with Tukey's post-hoc analysis; 2 independent experiments. (H–I) N2A cells were transfected with siRNA against *Grn*. Levels of Ran (H) and TDP-43 (I) were quantified via Western blot 7 d after transfection. $n = 6$ wells/group; **, $P = 0.002$ (TDP-43); **, $P = 0.006$ (Ran); 2 independent experiments. (J) Living wild-type or *Grn* KO primary neurons transfected with GFP + empty vector (control) or GFP + Ran were imaged longitudinally by automated microscopy at 24–48-h intervals for 7–9 d. Kaplan-Meir survival analysis was used to create cumulative risk of death functions for each population of transfected neurons. ***, $P < 0.001$ (log-rank test); $n = 423$ neurons (WT Ctrl), 518 neurons (KO Ctrl), 427 neurons (WT Ran), and 463 neurons (KO Ran); 3 independent experiments pooled. (K) Primary cortical neurons from wild-type or *Grn* KO mice were transduced with AAV-GFP (control) or AAV-GFP-P2A-Ran. 1 wk later, neurons were fixed and processed for TDP-43 immunostaining. Nuclear TDP-43 levels were quantified via Volocity. $n = 101$–478 cells imaged from 6–12 wells of a 96-well dish; *, $P < 0.05$ (mixed-effects multivariate linear regression model); 3 independent experiments. Means ± SEM shown (B, D, E, G–I, and K).

of TDP-43 in the retinas of *Grn* KO mice (Fig. 3 A). These findings suggest that nuclear depletion of TDP-43 in progranulin-deficient neurons could down-regulate Ran.

Ran is required for nuclear transport of the majority of proteins that shuttle between the nucleus and cytoplasm (Stewart, 2007). To determine if inactivation of Ran is sufficient to cause

nuclear depletion of TDP-43, we expressed dominant–negative RanQ69L (which cannot hydrolyze GTP) or RanT24N (which is nucleotide-free or GDP-bound) in cortical neurons. Both of these Ran mutants caused TDP-43 mislocalization (Fig. 4, F and G), indicating that TDP-43 requires functional Ran for import into the nucleus.

Enhancing Ran expression improves the survival of progranulin-deficient neurons

The results of the prior experiments suggested a model of a reciprocal depletion of nuclear TDP-43 and Ran: loss of nuclear TDP-43 down-regulates Ran mRNA, and Ran dysfunction depletes nuclear TDP-43. Indeed, acute knockdown of progranulin levels in N2A cells via siRNA reduced both TDP-43 and Ran protein expression (Fig. 4, H and I). To directly test this model, we hypothesized that augmenting Ran expression would increase nuclear TDP-43 and improve the survival of *Grn*-KO neurons. An automated microscopy approach was used to quantify the effect of Ran expression on neuron survival (Arrasate and Finkbeiner, 2005). In this assay, individual GFP-transfected neurons are repeatedly imaged over multiple days, thus generating longitudinal survival curves for cohorts of neurons from different genetic backgrounds and/or those expressing different plasmids. Previous studies have established that progranulin-deficient cortical neurons exhibit enhanced vulnerability in culture (Guo et al., 2010; De Muynck et al., 2013). Indeed, primary *Grn*-KO cortical neurons had shorter lives than wild-type neurons (Fig. 4 J). Expression of exogenous Ran enhanced the survival of *Grn*-KO neurons, but not wild-type neurons (Fig. 4 J). Consistent with our findings in the retina of *Grn*-KO mice, primary *Grn*-KO cortical neurons had decreased nuclear TDP-43 expression, which was increased by expression of exogenous Ran (Fig. 4 K).

In conclusion, our findings provide strong evidence of early retinal abnormalities in *GRN* mutation carriers. Retinal thinning occurred in cognitively asymptomatic GRN mutation carriers (who are at high risk for future dementia), indicating that retinal neuron loss is an early phenomenon that can precede clinical symptoms in FTD. Because small changes in retinal thickness can be reproducibly measured longitudinally via OCT, retinal imaging could be a useful modality for assessing response to therapeutics in early disease stages of progranulin-deficient FTD. Further study will be needed to establish the rate of retinal degeneration in *GRN* mutation carriers. The reasons why RGCs are particularly susceptible to death in *GRN* mutation carriers are unclear. RGCs have long axons and due to their central role in vision they have a high metabolic demand; both of these characteristics may contribute selective vulnerability in the setting of progranulin deficiency.

We also observed a retinal neurodegenerative phenotype in *Grn*-KO mice that parallels our observations in humans, establishing the retina as a new model system in which to study mechanisms of neurodegeneration in FTLD-TDP. Our findings support a pathogenic loop involving reciprocal depletion of nuclear TDP-43 and Ran as a potential mechanism of neurodegeneration in FTLD-TDP. In this model, loss of function of TDP-43 via nuclear depletion contributes to neurodegeneration and can occur without cytoplasmic TDP-43 aggregation. Loss of Ran expression, potentially in combination with other associated nuclear transport factors, impairs transport of TDP-43 to the nucleus (Nishimura et al., 2010). In turn, loss of nuclear TDP-43 lowers Ran levels, which could further deplete nuclear TDP-43. These data may point toward novel therapeutic strategies aimed at restoring nucleocytoplasmic transport as a means to improve neuronal survival in neurodegenerative diseases.

MATERIALS AND METHODS

Human subjects. Subjects enrolled through the UCSF Memory and Aging Center in whom *GRN* mutations were identified and age- and sex-matched control subjects without a history of neurological disease were invited to participate in our study. A standardized clinical evaluation was performed on all *GRN* mutation carriers at the UCSF Memory and Aging Center by board-certified neurologists who had additional training in behavioral neurology. For *GRN* mutation carriers, based on the results of this clinical evaluation, subjects were then subgrouped into asymptomatic *GRN* mutation carriers (CDR = 0, $n = 7$) and symptomatic *GRN* mutation carriers (CDR ≥ 0.5, $n = 5$). One *GRN* mutation carrier had a prior diagnosis of age-related macular degeneration. This subject was included in the analysis (exclusion of this subject from analysis did not meaningfully affect statistical significance of RNFL thinning or macular volume loss). No other control subjects or *GRN* mutation carriers had a history of ophthalmological disease or ocular surgery.

Written informed consent was obtained from all participants with capacity. Written informed consent was obtained from a designated surrogate decision maker in subjects deemed unable to provide informed consent due to diminished capacity, but we only enrolled subjects who were able to assent. The UCSF Committee on Human Research (CHR) approved this protocol, and the study was performed in accordance with the Declaration of Helsinki.

Retinal imaging. We performed spectral domain optical coherence tomography (OCT) at the UCSF Neurodiagnostics Center using a Heidelberg Spectralis instrument (Heidelberg Engineering, Heidelberg, Germany). A trained technician blinded to patient diagnosis and to genotype (when relevant) performed all scans and repeated each measurement at least three times. Mean RNFL thickness was determined using a peripapillary B-scan 3.4-mm from the center of the papilla. Images were evaluated by a blinded technician to meet prespecified image quality criteria, including signal intensity and beam uniformity. For this analysis, we analyzed and averaged the RNFL thickness and macular volume of all interpretable scans. RNFL thickness and macular volume was measured using automated software provided by Heidelberg. Segmentation analysis of macular scans was then performed to determine the volume of individual neuronal layers via a proprietary, validated computerized algorithm (Heidelburg Engineering, Heidelburg, Germany). Layers analyzed included the ganglion cell complex (GCC; comprising ganglion cell neuronal cell bodies, their dendrites, and axons projecting from underlying inner nuclear layer neurons), the inner nuclear layer (INL), and the outer nuclear layer (ONL).

Statistical analysis for human subjects. RNFL thickness, macular volumes, and segmented macular volume were analyzed in human subjects. We used multiple linear regression analysis to compare differences between *GRN* mutation carriers and unaffected controls. Adjustment for age and sex did not meaningfully change the results, so we elected to report unadjusted values. To account for inter-eye correlations, when two eyes from the same individual were analyzed, the standard error was adjusted using the clustered

sandwich estimator. $P < 0.05$ was considered significant. Analyses were performed using STATA 12.0.

Mice. Wild-type and *Grn*-KO mice were obtained from R.V. Farese's laboratory (University of California, San Francisco, CA; Martens et al., 2012). Mice used in experiments shown in Figs. 1–3 were of a mixed background consisting of 62.5% C57BL/6J, 12.5% 129Sv/Jae, and 25% FVB. Mice used in experiments shown in Fig. 4 were fully backcrossed into C57BL/6J. Age- and sex-matched mice from the same genetic background were used as controls for *Grn* KO mice.

RNFL and GCL neuron quantification. 16-µm transverse sections of WT and *Grn*-KO mouse eyes were made and stained with H&E/Neu-N, and the center sections (as determined by the center of the optic nerve head) were imaged via light/fluorescent microscopy, respectively. The area of the RNFL was measured in ImageJ and divided by the length of the RNFL across the field of view to determine thickness (equidistant from the optic nerve head across mice). For GCL neuron quantification, sections were stained with anti-NeuN antibody and subsequently imaged via fluorescence microscopy. The number of Neu-N positive cells in the GCL in individual fields of view were counted and divided by the length of the GCL using sections equidistant from the optic nerve head across mice. Statistical analysis was conducted with a one-way ANOVA followed by Tukey multiple comparison test.

Electroretinography. After overnight dark adaptation, mice were anesthetized under dim red illumination with 0.1 mg/kg ketamine and 10 mg/kg xylazine. Under anesthesia, both eyes were treated with 0.5% proparacaine followed by a mixture of 2.5% phenylephrine and 1% tropicamide for pupil dilation. The mice were kept warm using a 37°C heating pad (Deltaphase Isothermal Pads; Braintree Scientific). A gold reference electrode was electrically connected to the cornea of one eye and a platinum wire, mounted on a fiber-optic cable, was connected to the cornea of the other eye. Electrical continuity was made using hydroxypropyl methylcellulose (Goniosol). Light stimuli were delivered directly into the eye through the tip of the fiber optic. Stimulus intensity was controlled by calibrated neutral density filters, and stimulus wavelength was 500 nm (±5 nm; narrow band filter) or 505 nm (±17 nm; broad band filter). Responses were recorded from threshold up to light 1,000,000 fold brighter in darkness, and the photopic responses were recorded in the presence of rod-saturating background lights. Electrical responses were amplified (Astro-med CP122W; DC-300Hz) and digitized at 2 KHz (Real-Time PXI Computer; National Instruments).

Antibodies used. Rabbit anti-TDP-43 (Protein Tech), 1:1,000; rabbit C-terminal anti–TDP-43 (produced by G. Yu; UT Southwestern, Dallas, TX), 1:1,000 each; goat anti-Ran (Santa Cruz Biotechnology, Inc.), 1:200; and mouse anti-Ran (BD), 1:250–1:1,000.

Immunostaining. 16-µm transverse sections of WT and *Grn*-KO mouse eyes were made from paraffin embedded tissue and mounted on silanized slides. After de-waxing and rehydration, sections were blocked for 1 h at room temperature in PBS/0.5% Triton/10% donkey serum. Primary antibodies were incubated with sections overnight at 4°C, and then slides were washed and stained with secondary Alexa Fluor–conjugated antibodies (1:300; Invitrogen) for 2 h at room temperature. After washing, samples were mounted with #1.5 coverslips using Prolong-Gold antifade reagent with DAPI (Invitrogen). All fluorescent imaging was performed on an inverted confocal Ti microscope (Eclipse; Nikon) with a Nipkow spinning disk attachment and EM camera (Hamamatsu).

Quantification of TDP-43 and Ran. Sections from equal retinal eccentricity were imaged with a spinning disk confocal microscope, and fields of view of a similar distance from the center of the retinal sections were imaged. Acquisition settings were identical between samples, and all samples used for quantification were stained on the same day. Regions of interest were drawn around the DAPI-stained nuclei at the z-position center of the nuclei, and used to quantify mean intranuclear TDP-43 intensity. Cytoplasmic intensity of TDP-43 was determined by drawing a perinuclear region of interest in the cytoplasm. This mode of cytoplasmic intensity quantification was found to be more accurate than tracing around the entire cell soma, given the relatively high density of ganglion cells. Nuclear/cytoplasmic intensity ratios represent the mean nuclear intensity/mean cytoplasmic intensity per cell. For Ran quantification, intranuclear intensity was determined by drawing a ROI slightly inside of the nuclear envelope. Data were transformed into $\log_{10}$ intensity, and a mixed-model regression of the intensity variable versus genotype and/or age that controlled for clustering by mouse was applied to assess statistical significance in STATA.

Transfection of cortical neurons with Ran mutants. Postnatal day 0 rat cortical neurons were isolated and cultured in Neurobasal-A with B27. 3–5 d after isolation, they were transfected with human TDP-43-GFP + mCherry, mCherry-huRan, mCherry-huRanT24N, or mCherry-huRanQ69L. 1 d after transfection, neurons were fixed and imaged on a spinning disk confocal microscope. Images of mCherry-positive neurons were taken with the same acquisition settings across transfection groups, and the TDP-43-GFP signal in the nucleus and cytoplasm was quantified. Differences in nuclear/cytoplasmic ratio across groups was assessed with one-way ANOVA with Tukey's post-hoc analysis.

Immunostaining of postmortem brains from human subjects with *GRN* mutations. De-identified post-mortem brain tissue (left inferior frontal gyrus) from FTLD subjects with previously documented *GRN* mutations, deemed nonhuman subject material as per UCSF CHR guidelines, was obtained from the UCSF Neurodegenerative Disease Brain Bank. Tissue was embedded in paraffin and 10-µm sections were made. Antigen retrieval was performed using IHC World's antigen retrieval solution as per manufacturer's guidelines, followed by Sudan Black treatment and primary antibody incubation overnight at 4°C (anti–TDP-43, 1:3,000; Protein Tech; anti-Ran, 1:1,000; BD), followed by secondary antibody and DAPI-staining. For quantification of staining, confocal images of DAPI-stained nuclei, TDP-43, and Ran were taken at equal intensities across multiple fields of view in the cortex. Nuclear TDP-43 and Ran levels were quantified and analyzed as was done in mouse RGCs.

TDP-43 RIP. The TDP-43-RNA immunoprecipitation dataset was generated from pull-down experiments conducted as part of a previous study using the methods described therein (Sephton et al., 2011).

TDP-43 knockdown, progranulin knockdown, Q-RT-PCR, and Western blot analysis. N2A cells were grown in DMEM (low glucose) + 10% FCS and transfected with Mission TDP-43 shRNA construct #752 or control shRNA construct (Sigma-Aldrich) via Lipofectamine 2000. 6–8 d after transfection, N2A cells were harvested for RNA or protein analysis. RNA was prepared via RNeasy columns (QIAGEN), transcribed into cDNA, and Ran or cyclophilin (control) RNA levels were analyzed via Q-RTPCR. Equal amounts of total protein from knockdown and control cells were immunoblotted against tubulin (loading control), TDP-43, or Ran, and then quantified using a Licor imaging system, with relative levels of Ran/tubulin quantified for each sample. For progranulin knockdown experiments, N2A cells were transfected with control siRNA (Thermo Fisher Scientific) or Grn#1 siRNA. Greater than 95% knockdown was observed by Western blot and progranulin ELISA by 5 d after transfection. Samples were processed for Ran and TDP-43 quantification, as above. For Ran mRNA analysis of mouse retinas, whole retinas were isolated from freshly perfused mice and nonneuroretinal tissue was dissected away. RNA preparation and Q-RTPCR was performed as above.

Longitudinal neuronal survival analysis. Longitudinal survival analysis of individual GFP-transfected neurons was essentially performed as described previously (Barmada et al., 2010), with the following modifications: cortical

neurons from postnatal day 0 wild-type or Grn KO mice were dissociated and plated on PDL-coated 96 well-dishes (microclear bottom dishes; Greiner) at a density of 90,000 cells/well in Neurobasal-A + B27 supplement. 3–5 d after plating, neurons were transfected via Lipofectamine 2000 with GFP + empty vector or GFP + mouse Ran cDNA at a ratio of 1:3 to ensure that all fluorescent cells co-expressed the second plasmid. The day after transfection, wells containing GFP-expressing neurons were imaged at 5× magnification with an automated microscope (Array Scanner XTI; Thermo Fisher Scientific). The same fields of view were reimaged every 24–48 h for a total of 7–9 d after transfection. Adjacent fields of view from individual wells were stitched together into montages via ImageJ, and a time series across days for each well was then generated using a custom-made macro in ImageJ. The survival of individual GFP-transfected neurons over time was then assessed by loss of GFP fluorescence. Kaplan-Meier and cumulative risk of death curves were made with R software, and statistical significance of differences in survival between cohorts of neurons was determined with the log-rank test. Tukey multiple comparison test was used for comparisons involving more than two groups.

Rescue of neuronal TDP-43 expression. Primary cortical neurons from postnatal day 0 wild-type or Grn KO pups were isolated and plated as described above. Neurons were transduced with AAV2-GFP (Virovek) or AAV2-GFP-P2A-human Ran (in which bicistronic GFP and untagged Ran co-expression is driven by a single chicken-β-actin-CMV promoter, with a P2A sequence separating GFP and Ran sequences). 7 d after transduction, neurons were fixed and immunostained with anti–TDP-43 antibody. Individual wells were imaged, and regions of interest of nuclei from GFP-positive cells were generated via Volocity from background-subtracted images. Using these regions of interest, integrated density measurements of total TDP-43 levels in each nuclei were then calculated. A mixed-model regression of the intensity variable versus genotype and AAV-vector that controlled for clustering by well was applied to assess statistical significance in STATA.

Statistics. Design and execution of statistical tests were done in collaboration with a professional biostatistician (J. Boscardin, University of California, San Francisco, CA). For human retinal imaging data and for nuclear and cytoplasmic TDP-43 and Ran immunostaining in retinal neurons and in cultured cortical neurons, significance was determined via mixed-effects linear regression analyses, accounting for interindividual, within-eye correlations in the human studies and intramouse clustering in rodent models. In experiments involving two comparison groups, unpaired two-tailed Student's *t* tests were used to assess for differences. In experiments involving more than two comparison groups, ANOVA test with post-hoc tests (Tukey or Bonferroni, as specified in the text) were used. For longitudinal neuronal survival analysis, cumulative risk of death curves were generated with R software, and statistical significance was determined with the log-rank test. $P < 0.05$ was considered significant. Unless otherwise noted, statistical testing was performed using Prism and Stata 12.0 software.

Study approval. For retinal imaging, written informed consent was obtained from all participants with capacity; in subjects deemed unable to provide informed consent due to diminished capacity, written consent was obtained from a designated surrogate decision-maker and subjects provided assent. The study protocol was approved by the UCSF Committee on Human Research (IRB # 11–05333). For studies involving mice, all procedures were approved by the Institutional Animal Care and Use Committee at UCSF (#AN087501-02A) and UAB (#101109282, #130309617).

Online supplemental material. Fig. S1 shows clinical characteristics of human subjects who underwent retinal imaging. Online supplemental material is available at http://www.jem.org/cgi/content/full/jem.20140214/DC1.

We would like to thank Dr. Sami Barmada for his thoughtful input on the project and assistance with analysis of neuronal survival experiments, Yungui Zhou and Marcel Alavi for technical assistance, Dr. Anna Karydas for her assistance with genetic analysis of human subjects, and Dr. Laura Mitic for her feedback.

This project was funded by the Consortium for Frontotemporal Dementia Research (L.G., G.Y., E.D.R. J.H., B.V.F), The Bluefield Project to Cure FTD (M.W., fellowship), R01 AG036884 (L.G), the UCSF Resource Allocation Program (A.G.), the UCSF Alzheimer's Disease Research Center (M.W.), #P50 AG023501 (B.F), R01NS079796 (G.Y.), R01NS075487 (E.D.R), T32HD071866 (A.E.A), K08EY023610, (M.W) the Chartrand Foundation and Clinical & Science Translational Institute (M.W., A.G.), the Howard Hughes Medical Institute (A.G.), the Alzheimer's Association (G.Y.), the Welch Foundation (G.Y.), R37HL63762 (J.H), the Brightfocus Foundation (J.H), the Alzheimer's Drug Discovery Foundation (B.M).

The authors report no competing financial interests.

Submitted: 31 January 2014
Accepted: 5 August 2014

REFERENCES

Ahmed, Z., H. Sheng, Y.-F. Xu, W.-L. Lin, A.E. Innes, J. Gass, X. Yu, C.A. Wuertzer, H. Hou, S. Chiba, et al. 2010. Accelerated lipofuscinosis and ubiquitination in granulin knockout mice suggest a role for progranulin in successful aging. *Am. J. Pathol.* 177:311–324. http://dx.doi.org/10.2353/ajpath.2010.090915

Albrecht, P., A.-K. Müller, M. Südmeyer, S. Ferrea, M. Ringelstein, E. Cohn, O. Aktas, T. Dietlein, A. Lappas, A. Foerster, et al. 2012. Optical coherence tomography in parkinsonian syndromes. *PLoS ONE.* 7:e34891. http://dx.doi.org/10.1371/journal.pone.0034891

Arnold, E.S., S.-C. Ling, S.C. Huelga, C. Lagier-Tourenne, M. Polymenidou, D. Ditsworth, H.B. Kordasiewicz, M. McAlonis-Downes, O. Platoshyn, P.A. Parone, et al. 2013. ALS-linked TDP-43 mutations produce aberrant RNA splicing and adult-onset motor neuron disease without aggregation or loss of nuclear TDP-43. *Proc. Natl. Acad. Sci. USA.* 110:E736–E745. http://dx.doi.org/10.1073/pnas.1222809110

Arrasate, M., and S. Finkbeiner. 2005. Automated microscope system for determining factors that predict neuronal fate. *Proc. Natl. Acad. Sci. USA.* 102:3840–3845. http://dx.doi.org/10.1073/pnas.0409777102

Baker, M., I.R. Mackenzie, S.M. Pickering-Brown, J. Gass, R. Rademakers, C. Lindholm, J. Snowden, J. Adamson, A.D. Sadovnick, S. Rollinson, et al. 2006. Mutations in progranulin cause tau-negative frontotemporal dementia linked to chromosome 17. *Nature.* 442:916–919. http://dx.doi.org/10.1038/nature05016

Barmada, S.J., G. Skibinski, E. Korb, E.J. Rao, J.Y. Wu, and S. Finkbeiner. 2010. Cytoplasmic mislocalization of TDP-43 is toxic to neurons and enhanced by a mutation associated with familial amyotrophic lateral sclerosis. *J. Neurosci.* 13:639–649. http://dx.doi.org/10.1523/JNEUROSCI.4988-09.2010

Bayer, A.U., O.N. Keller, F. Ferrari, and K.-P. Maag. 2002. Association of glaucoma with neurodegenerative diseases with apoptotic cell death: Alzheimer's disease and Parkinson's disease. *Am. J. Ophthalmol.* 133:135–137. http://dx.doi.org/10.1016/S0002-9394(01)01196-5

Chen-Plotkin, A.S., F. Geser, J.B. Plotkin, C.M. Clark, L.K. Kwong, W. Yuan, M. Grossman, V.M. Van Deerlin, J.Q. Trojanowski, and V.M.-Y. Lee. 2008. Variations in the progranulin gene affect global gene expression in frontotemporal lobar degeneration. *Hum. Mol. Genet.* 17:1349–1362. http://dx.doi.org/10.1093/hmg/ddn023

Davidson, Y., T. Kelley, I.R.A. Mackenzie, S. Pickering-Brown, D. Du Plessis, D. Neary, J.S. Snowden, and D.M.A. Mann. 2007. Ubiquitinated pathological lesions in frontotemporal lobar degeneration contain the TAR DNA-binding protein, TDP-43. *Acta Neuropathol.* 113:521–533. http://dx.doi.org/10.1007/s00401-006-0189-y

De Muynck, L., S. Herdewyn, S. Beel, W. Scheveneels, L. Van Den Bosch, W. Robberecht, and P. Van Damme. 2013. The neurotrophic properties of progranulin depend on the granulin E domain but do not require sortilin binding. *Neurobiol. Aging.* 34:2541–2547. http://dx.doi.org/10.1016/j.neurobiolaging.2013.04.022

Guo, A., L. Tapia, S.X. Bamji, M.S. Cynader, and W. Jia. 2010. Progranulin deficiency leads to enhanced cell vulnerability and TDP-43 translocation in primary neuronal cultures. *Brain Res.* 1366:1–8. http://dx.doi.org/10.1016/j.brainres.2010.09.099

Helmer, C., F. Malet, M.-B. Rougier, C. Schweitzer, J. Colin, M.-N. Delyfer, J.-F. Korobelnik, P. Barberger-Gateau, J.-F. Dartigues, and C. Delcourt. 2013. Is there a link between open-angle glaucoma and

dementia? The 3C-alienor cohort. *Ann. Neurol.*:n/a. http://dx.doi.org/10.1002/ana.23926

Hinton, D.R., A.A. Sadun, J.C. Blanks, and C.A. Miller. 1986. Optic-nerve degeneration in Alzheimer's disease. *N. Engl. J. Med.* 315:485–487. http://dx.doi.org/10.1056/NEJM198608213150804

Igaz, L.M., L.K. Kwong, E.B. Lee, A. Chen-Plotkin, E. Swanson, T. Unger, J. Malunda, Y. Xu, M.J. Winton, J.Q. Trojanowski, and V.M.-Y. Lee. 2011. Dysregulation of the ALS-associated gene TDP-43 leads to neuronal death and degeneration in mice. *J. Clin. Invest.* 121:726–738. http://dx.doi.org/10.1172/JCI44867

Koronyo-Hamaoui, M., Y. Koronyo, A.V. Ljubimov, C.A. Miller, M.K. Ko, K.L. Black, M. Schwartz, and D.L. Farkas. 2011. Identification of amyloid plaques in retinas from Alzheimer's patients and noninvasive in vivo optical imaging of retinal plaques in a mouse model. *Neuroimage.* 54(Suppl 1):S204–S217. http://dx.doi.org/10.1016/j.neuroimage.2010.06.020

Lee, E.B., V.M.-Y. Lee, and J.Q. Trojanowski. 2012. Gains or losses: molecular mechanisms of TDP43-mediated neurodegeneration. *Nat. Rev. Neurosci.* 13:38–50.

Martens, L.H., J. Zhang, S.J. Barmada, P. Zhou, S. Kamiya, B. Sun, S.-W. Min, L. Gan, S. Finkbeiner, E.J. Huang, and R.V. Farese Jr. 2012. Progranulin deficiency promotes neuroinflammation and neuron loss following toxin-induced injury. *J. Clin. Invest.* 122:3955–3959. http://dx.doi.org/10.1172/JCI63113

Melchior, F., T. Guan, B. Paschal, and L. Gerace. 1995. Biochemical and structural analysis of nuclear protein import. *Cold Spring Harb. Symp. Quant. Biol.* 60:707–716. http://dx.doi.org/10.1101/SQB.1995.060.01.077

Neumann, M., D.M. Sampathu, L.K. Kwong, A.C. Truax, M.C. Micsenyi, T.T. Chou, J. Bruce, T. Schuck, M. Grossman, C.M. Clark, et al. 2006. Ubiquitinated TDP-43 in frontotemporal lobar degeneration and amyotrophic lateral sclerosis. *Science.* 314:130–133. http://dx.doi.org/10.1126/science.1134108

Nishimura, A.L., V. Zupunski, C. Troakes, C. Kathe, P. Fratta, M. Howell, J.M. Gallo, T. Hortobágyi, C.E. Shaw, and B. Rogelj. 2010. Nuclear import impairment causes cytoplasmic trans-activation response DNA-binding protein accumulation and is associated with frontotemporal lobar degeneration. *Brain.* 133:1763–1771. http://dx.doi.org/10.1093/brain/awq111

Paquet, C., M. Boissonnot, F. Roger, P. Dighiero, R. Gil, and J. Hugon. 2007. Abnormal retinal thickness in patients with mild cognitive impairment and Alzheimer's disease. *Neurosci. Lett.* 420:97–99. http://dx.doi.org/10.1016/j.neulet.2007.02.090

Polymenidou, M., C. Lagier-Tourenne, K.R. Hutt, S.C. Huelga, J. Moran, T.Y. Liang, S.-C. Ling, E. Sun, E. Wancewicz, C. Mazur, et al. 2011. Long pre-mRNA depletion and RNA missplicing contribute to neuronal vulnerability from loss of TDP-43. *Nat. Neurosci.* 14:459–468. http://dx.doi.org/10.1038/nn.2779

Sephton, C.F., C. Cenik, A. Kucukural, E.B. Dammer, B. Cenik, Y. Han, C.M. Dewey, F.P. Roth, J. Herz, J. Peng, et al. 2011. Identification of neuronal RNA targets of TDP-43-containing ribonucleoprotein complexes. *J. Biol. Chem.* 286:1204–1215. http://dx.doi.org/10.1074/jbc.M110.190884

Stewart, M. 2007. Molecular mechanism of the nuclear protein import cycle. *Nat. Rev. Mol. Cell Biol.* 8:195–208. http://dx.doi.org/10.1038/nrm2114

Tamura, H., H. Kawakami, T. Kanamoto, T. Kato, T. Yokoyama, K. Sasaki, Y. Izumi, M. Matsumoto, and H.K. Mishima. 2006. High frequency of open-angle glaucoma in Japanese patients with Alzheimer's disease. *J. Neurol. Sci.* 246:79–83. http://dx.doi.org/10.1016/j.jns.2006.02.009

Wegorzewska, I., and R.H. Baloh. 2011. TDP-43-based animal models of neurodegeneration: new insights into ALS pathology and pathophysiology. *Neurodegener. Dis.* 8:262–274. http://dx.doi.org/10.1159/000321547

Yin, F., M. Dumont, R. Banerjee, Y. Ma, H. Li, M.T. Lin, M.F. Beal, C. Nathan, B. Thomas, and A. Ding. 2010. Behavioral deficits and progressive neuropathology in progranulin-deficient mice: a mouse model of frontotemporal dementia. *FASEB J.* 24:4639–4647. http://dx.doi.org/10.1096/fj.10-161471